Progress In Electromagnetics Research, Vol. 122, 557–575, 2012

A TIME-DOMAIN APPROACH TO THE SYNTHESIS OF UWB ANTENNA SYSTEMS

L. Lizzi, G. Oliveri, and A. Massa*

ELEDIA Research Center, Department of Information Engineering and Computer Science, University of Trento, Via Sommarive 14, Trento 38050, Italy

Abstract—In this paper, an approach for the synthesis of Ultra-Wideband (UWB) antenna systems in the time domain is proposed. Starting from the definition of suitable time-domain performance indexes, the design process is based on a spline representation of the antenna shape and a Particle Swarm Optimization (PSO) aimed at matching optimal radiation and electrical conditions. The effectiveness of the proposed time-domain technique is assessed by means of both numerical and experimental results.

1. INTRODUCTION

In Ultra-Wideband (UWB) communication systems, the information is transmitted by means of very short time pulses to enable high data-rate communications, low complexity and costs, resistance to severe multipath, and a suitable time-domain resolution for localization and tracking purposes [1]. In order to yield these features, the design of reliable UWB antennas is usually a very demanding task and the quality of the transmitted and received signals is an issue to be carefully taken into account [2, 3].

Antenna systems are generally analyzed in the frequency domain and their electrical properties are described in terms of frequency-dependent parameters (e.g., efficiency, input impedance, gain, effective area, polarization properties, and radiation patterns) [3–6]. Dealing with narrowband signals, the antenna properties can be profitably analysed at the center-band frequency to provide a comprehensive description. For wider bandwidths, the dependence on the frequency

Received 30 October 2011, Accepted 1 December 2011, Scheduled 8 December 2011

* Corresponding author: Andrea Massa (andrea.massa@ing.unitn.it).

cannot be neglected [6]. In such a framework, several approaches have been proposed in the last years. In [7, 8], the synthesis process is carried out through a parametric study aimed at obtaining a good impedance matching within the UWB band. Similarly, an approach for designing semi-elliptical UWB antennas is discussed in [9]. The proposed method exploits some simple design equations to minimize the antenna return loss in a very large bandwidth. Also the authors of this paper proposed a technique based on a Particle Swarm Optimizer (PSO) for synthesizing UWB spline-shaped antennas with a good impedance matching and distortionless behaviour [10].

Although easy, expressing the antenna properties as a function of frequency unavoidably compromises their compactness and simplicity [11]. Moreover, a frequency-by-frequency analysis of very short duration UWB pulses (i.e., a very large bandwidth in the frequency domain) is quite inefficient and generally time-consuming [12]. Therefore, it seems to be more convenient to analyse UWB systems in the time domain [13, 14] by defining some useful counterparts of the standard frequency-based antenna parameters [11, 12, 15–17]. An example of a design procedure partially performed in the time domain can be found in [18], where a genetic-based optimization of a simplified version of the volcano smoke antenna is described. More specifically, the synthesis is devoted to minimize the antenna return loss (a frequency-domain parameter), while maximizing the correlation factor (a time-domain parameter). The same approach has been successfully exploited for designing planar differential elliptical UWB antennas [19]. Similar approaches can be found in [6, 8, 20].

In this paper, a full time-domain approach to the synthesis of UWB antennas is presented. Towards this end, the synthesis requirements for efficient UWB communications are conveniently formulated in time-domain by still enforcing that the antenna is able to radiate as much energy as possible, but with stronger constraints because of the low energy associated to UWB pulses. Moreover, the radiation properties are optimized to show an omnidirectional behavior over the whole working frequency band. Successively, the antenna descriptors are optimized [10] to fit the design requirements with an iterative procedure based on a PSO [21–24] and on a spline representation [25] of the radiating structure. It is worth noticing that unlike [10] the analysis is here carried out entirely in the time-domain by optimizing the radiation properties of the prototype under test, as well.

Thanks to the full time-domain analysis, the spline-based geometry representation and the PSO-based optimization, the

proposed antenna synthesis approach provides a number of advantages with respect to other classical design procedures. First of all, dealing with UWB signals characterized by several GHz bandwidth, the characterization of the antenna performances in the time-domain is faster and more accurate than evaluating electrical and radiating parameters over a large set of frequency points, as usually done by standard frequency-domain synthesis approaches. Moreover, the representation of the antenna geometry by means of spline curves provides two main advantages. With respect to parametric design techniques (e.g., as in [26, 27]), where a reference shape for the antenna structure is a-priori fixed, the proposed method provides flexibility in generating widely different stuctures. On the other hand, with respect to the so-called building-block design technique (e.g., as in [28, 29]), where the antenna structure is obtained by properly combining a number of elementary blocks, the proposed approach allows the geometry description by means of a reduced number of parameters. These two aspects are fundamental in order to obtain an effective synthesis procedure. Numerical results showing the effectiveness of the spline-based method in comparison to the parametric and the building-block approaches are reported in [10] and [30], respectively. Thanks to these positive features, the proposed method results to be more attractive when the project requirements are particulary hard to fulfil.

The paper is organized as follows. Section 2 discusses the antenna characteristics in the time domain to define the key UWB requirements for the full time-domain design process. The synthesis approach is then presented in Section 3, while Section 4 is devoted to assess the proposed approach by means of some numerical and experimental validations. Finally, some conclusions are reported in Section 5.

2. TIME DOMAIN ANALYSIS

With reference to a simple UWB communication system composed by a pair of two identical antennas at a distance d from each other (Fig. 1), the transmitted UWB waveform $u(t)$ is received as an output signal $v(t)$ potentially corrupted because of the non-ideal behavior of both radiators and transmission channel. To avoid or minimize such a drawback, the whole system and in particular the antennas must be properly designed in order to fit the set of requirements defined in the following. First, the ideal transmitting antenna is expected to radiate as much energy as possible. This is mathematically stated by defining the *antenna efficiency* E which, based on the signal energies [31], expresses the amount of the radiated energy with respect to the total

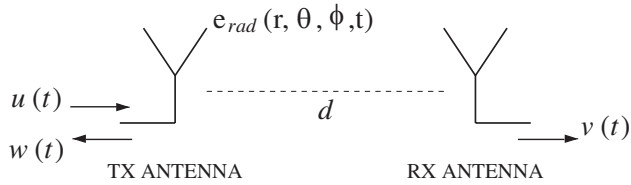

Figure 1. Sketch of a simplified UWB communication system.

input energy, i.e.,

$$E = 1 - \frac{\int_{-\infty}^{+\infty} |w(t)|^2 \, dt}{\int_{-\infty}^{+\infty} |u(t)|^2 \, dt} \tag{1}$$

where $w(t)$ is the reflected component of the input signal at the transmitting antenna. The antenna efficiency ranges in the interval of values $0 \leq E \leq 1$ and it tends to unity when the energy content of the reflected signal $w(t)$ goes to zero. In other words, higher values of E denote well-behaved systems enabling efficient and reliable communications.

On the other hand and besides the antenna efficiency, UWB systems must guarantee the non-distorted reception of the transmitted signal, as well. To quantify the distortion between the transmitted and the received signals, let us define the *system fidelity* index F

$$F = \max_{\tau} \int_{-\infty}^{+\infty} \hat{v}(t-\tau) \, \hat{u}(t) \, dt \tag{2}$$

equal to the maximum of the cross-correlation function [15]. In (2), $\hat{u}(t) = u(t)/\sqrt{\int_{-\infty}^{+\infty} |u(t)|^2 dt}$ and $\hat{v}(t) = v(t)/\sqrt{\int_{-\infty}^{+\infty} |v(t)|^2 dt}$ are normalized quantities with unitary energy. Concerning the meaning and the dynamic of F, it is constrained to the range [0, 1]. More specifically, the fidelity index is equal to zero when the transmitted and the received signals are different, while it assumes a unitary value when the received waveform is just an attenuated and delayed version of the transmitted one.

Finally, antennas for UWB communications are usually expected to have omnidirectional radiation patterns in a wide frequency bandwidth. In time domain, such a requirement can be recast into a condition on the the so-called *similarity factor* $S(\theta, \phi)$ that quantifies the change of the waveform shape of the radiated pulse versus the observation direction (θ, ϕ)

$$S(\theta, \phi) = 1 - \frac{\int_{-\infty}^{+\infty} |\mathbf{e}_{\mathrm{rad}}(r, \theta_0, \phi_0, t) - \mathbf{e}_{\mathrm{rad}}(r, \theta, \phi, t)|^2 \, dt}{\int_{-\infty}^{+\infty} |\mathbf{e}_{\mathrm{rad}}(r, \theta_0, \phi_0, t)|^2 \, dt} \tag{3}$$

$\mathbf{e}_{\text{rad}}(r, \theta, \phi, t)$ being the radiated electric field and (θ_0, ϕ_0) stands for the direction of the maximum radiation [16]. As it can be derived from (3), it turns out that $0 \leq S(\theta, \phi) \leq 1$ being $S(\theta_0, \phi_0) = 1$.

3. UWB ANTENNA SYNTHESIS

Starting from the definition of the time-domain parameters "quantifying" the efficiency and reliability of an UWB radiating systems, the synthesis process is recast as an optimization where each trial solution, $\mathbf{a}$, identifies an antenna geometry univocally described by a set of N geometric descriptors $\mathbf{a} = \{a_n;\ n = 1, \ldots, N\}$.

With reference to the geometry shown in Fig. 2 [10], the antenna is modeled as a microstrip structure composed by a radiating part defined by a spline curve and a metallic ground plane printed on a dielectric substrate. More specifically, α_1 and α_2 denote the length and one half of the width of the substrate, respectively, α_3 is one half of the feedline width, and α_4 is the length of the ground plane on the back side of the dielectric substrate. As for the spline contour of the radiating part, it is identified by I control points $\{P_i = (y_{pi}, z_{pi});\ i = 1, \ldots, I\}$. Unlike [10], also the ground plane is modeled with a spline curve [Fig. 5(b)] with J control points, $\{Q_j = (y_{qj}, z_{qj});\ j = 1, \ldots, J\}$. Consequently, the descriptive vector $\mathbf{a}$ is the collection of the geometric variables $\{\alpha_1, \ldots, \alpha_4\}$ and of the coordinates of the control points of

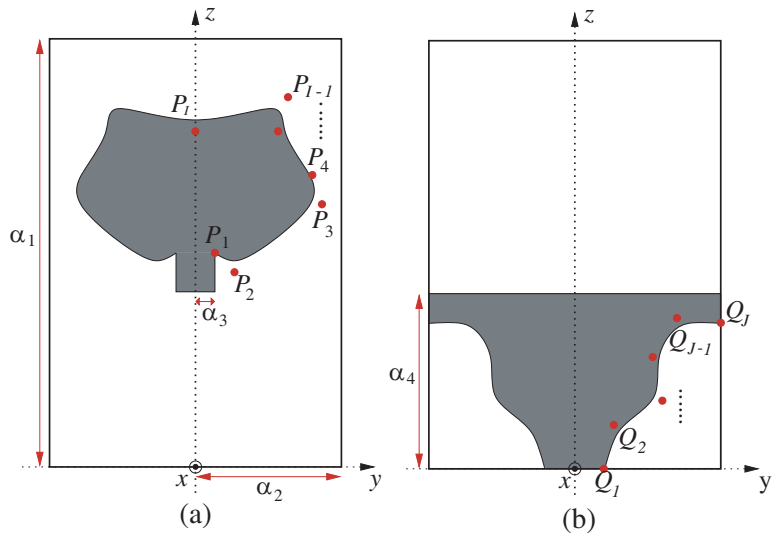

Figure 2. Reference antenna geometry.

the spline contours

$$\mathbf{a} = \{a_n;\, n = 1, \ldots, N\}\,, \quad N = 4 + (I + J)\,, \tag{4}$$

being $(a_n = \alpha_n,\ n = 1, \ldots, 4)$, $(a_{i+5} = P_i,\ i = 1, \ldots, I)$, and $(a_{j+I+6} = Q_j,\ j = 1, \ldots, J)$.

Because of the continuous variables to be determined, the optimization is carried out by means of a PSO-based algorithm that widely proved its efficiency in solving such a kind of problems [21, 32–34]. Accordingly, the synthesized solution $\mathbf{a}_{\text{opt}}$ turns out to be the trial set of parameters that minimizes a suitable cost function ξ

$$\mathbf{a}_{\text{opt}} = \arg\min_{\mathbf{a}} \left[\xi\left(\mathbf{a}\right)\right]. \tag{5}$$

Generally, the cost function ξ is the metric that mathematically quantifies the fitness of each trial solution to the problem at hand. In such a case, the value $\xi\left(\mathbf{a}\right)$ gives the compliance of the descriptors vector $\mathbf{a}$ to the design constraints. Therefore, ξ is here defined as the sum of three terms proportional to the performance indexes in Section 2

$$\xi\left(\mathbf{a}\right) = \xi_E\left(\mathbf{a}\right) + \xi_F\left(\mathbf{a}\right) + \xi_S\left(\mathbf{a}\right) \tag{6}$$

where $\xi_E\left(\mathbf{a}\right)$ and $\xi_F\left(\mathbf{a}\right)$ refer to the efficiency and the fidelity of the antenna

$$\xi_E(\mathbf{a}) = \max\left\{0, \frac{E^T - E}{E^T}\right\} \tag{7}$$

$$\xi_F(\mathbf{a}) = \max\left\{0, \frac{F^T - F}{F^T}\right\}, \tag{8}$$

while the superscript ^{T} stands for target value. Analogously, $\xi_S\left(\mathbf{a}\right)$ is concerned with the similarity index

$$\xi_S(\mathbf{a}) = \text{mean}_{\theta,\phi}\left\{\xi_S^{(\theta,\phi)}(\mathbf{a})\right\} \tag{9}$$

where

$$\xi_S^{(\theta,\phi)}(\mathbf{a}) = \max\left\{0, \frac{S^T(\theta,\phi) - S(\theta,\phi)}{S^T(\theta,\phi)}\right\}. \tag{10}$$

The antenna performances used to evaluate the cost function are computed by means of an in-house code based on the Finite Integration Technique (FIT) [35]. The iterative optimization procedure evolves according to the PSO strategy as detailed in [21, 24]. A swarm of R particles $\mathbf{a}_r^{(k)};\ r = 1, \ldots, R$ is randomly chosen at the initialization $k = 0$, k being the iteration index. Successively $(k > 0)$, the positions and the velocities of the particles sampling the solution space are updated [36] until a maximum number of iteration K is reached (i.e., $k = K$) or the fitness of a trial solution satisfies the following convergence criterion, $\xi\left(\mathbf{a}_r^{(k)}\right) \leq \eta$, η being a user-defined convergence threshold.

4. NUMERICAL AND EXPERIMENTAL VALIDATION

This section is aimed at presenting a set of numerical and experimental results to show the reliability as well as the effectiveness of the time-domain synthesis approach (Section 3). Two test cases, indicated as '*Test Case A*' and '*Test Case B*', will be analyzed and discussed as representative outcomes from the proposed method.

The first test case (*Test Case A*) deals with an UWB system of two identical antennas at a distance of $d = 15\,\text{cm}$ that transmits/receives an UWB input waveform of duration equal to about 1 ns with a corresponding bandwidth of 5 GHz from about 4 GHz up to 9 GHz. As far as the user requirements are concerned, both the antenna efficiency and the system fidelity target values have been set to $E^T = F^T = 0.95$, while the target similarity factor has been fixed to $S^T(\theta, \phi) = 0.95$ in the x-y plane ($\theta = 90°$) to give an omnidirectional behavior along the horizontal plane. Concerning the antenna geometry, the number of control points for the spline description has been chosen equal to $I = J = 7$ (i.e., $N = 32$) to yield a good trade-off between shape generality and number of unknowns (i.e., dimension of the solution space). Concerning the antenna sizing, the maximum dimension has been upper bounded to $50 \times 50\,\text{mm}^2$. The optimization has been carried out with the following setup: a population of $R = 5$ particles, a maximum number of iterations $K = 100$, and a convergence threshold equal to $\eta = 10^{-5}$. The entire optimization process took approximately four hours (about 30 seconds per particle per iteration) on a standard PC (Intel Core i5 at 3.2 GHz with 4 GB of memory).

Let us now analyse the optimization process by observing the evolution of both the antenna geometry and the antenna performance. Starting from an antenna configuration randomly generated (i.e., randomly selecting the spline control points), the optimization loop iteratively modifies the antenna descriptors to find the best solution fitting the user-defined requirements. The evolution of the variables $\{\alpha_1, \ldots, \alpha_4\}$ versus the iteration number is reported in Fig. 3, while the values of the coordinates of the control points are given in Fig. 4. As expected, the variations of the descriptors are generally more consistent at the beginning of the iterative process, while they reduce progressively until almost constant values at the convergence. As far as the antenna performance is concerned, Fig. 5 describes the iterative evolution of the optimal trial solution $\mathbf{a}_{\text{opt}}^{(k)}$ in terms of the corresponding cost function value, $\xi_{\text{opt}}^{(k)} = \xi(\mathbf{a}_{\text{opt}}^{(k)})$, and related terms. More in detail, the solid line and the dashed line refer to the antenna efficiency E term (1) and the system fidelity F term (2), respectively. Moreover, the dotted line gives the mean values of the similarity factor

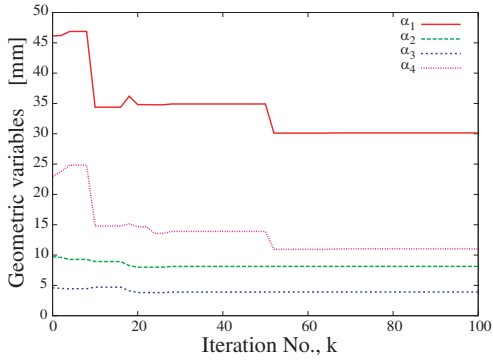

Figure 3. *Test Case A* — Evolution of the geometric variables $\{\alpha_1, \ldots, \alpha_4\}$

over all the angular directions, $S_m = \text{mean}_{\theta,\phi}\{S(\theta,\phi)\}$. As it can be observed, the whole set of UWB performance indexes improves during the optimization until a suitable fitting with the design objectives ($\xi_{\text{opt}}^{(K)} = 1.21 \times 10^{-5}$) is achieved at the convergence ($K = 100$). The result from the optimization is an antenna prototype with small dimensions (30.1×16.2 mm) as pointed out in Table 1 where the values of the optimized descriptors are given, as well. As for the temporal behaviour, Fig. 6 compares the input signal $u(t)$ and the reflected one $w(t)$. Because of the low amplitude as well as dynamic of the reflections, the synthesized antenna turns out to be very efficient in radiating the signal energy as confirmed by the corresponding efficiency index $E = 0.98$. The antenna effectiveness is further assessed by the value of the fidelity parameter ($F = 0.97$). In order to give some more indications about the fidelity issue, Fig. 7 plots the energy-normalized versions of the input and received signals [i.e., $\hat{v}(t)$ and $\hat{u}(t)$] to point out the close similarities as an indicator of the system reliability. Finally, the radiated electric field towards different azimuth directions and the resulting similarity factor are shown in Fig. 8. As required, the antenna shows an omnidirectional behavior along the horizontal plane by verifying the condition $S(\theta = 90°, \phi) \geq 0.95$.

For completeness, the prototype performances have been analyzed in the frequency domain, as well. Although redundant for assessing the antenna reliability because of the previous time-domain validation, the results of such a study are reported to give the reader the counterpart in the frequency of the time-domain parameters and an explanation/link in frequency of their meaning. Towards this end, the two-antenna system has been modeled as an equivalent two-port network and its

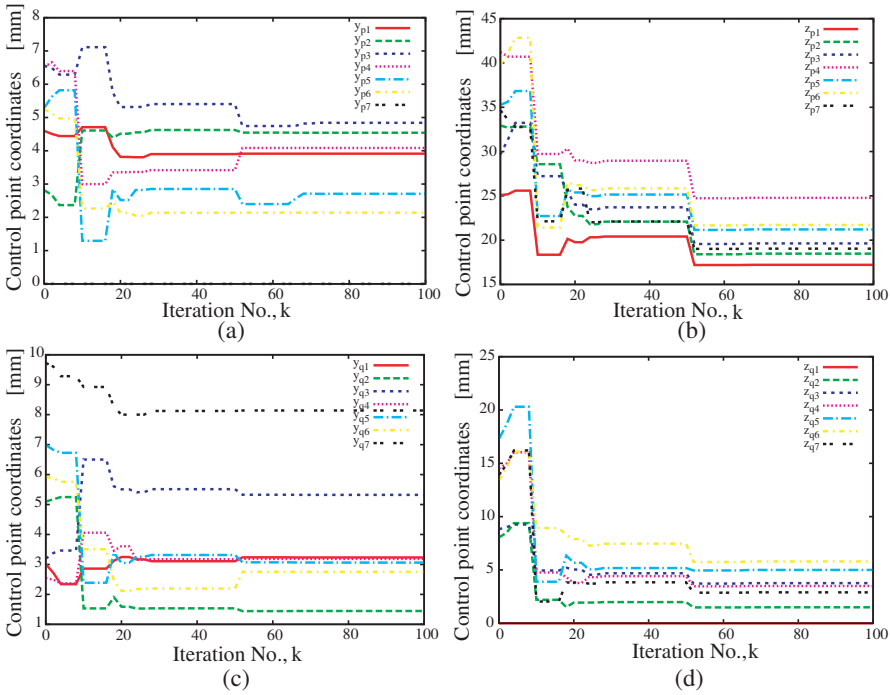

Figure 4. *Test Case A* — Evolution of the spline control points in (a) the radiating part and (b) the ground plane of the antenna geometry.

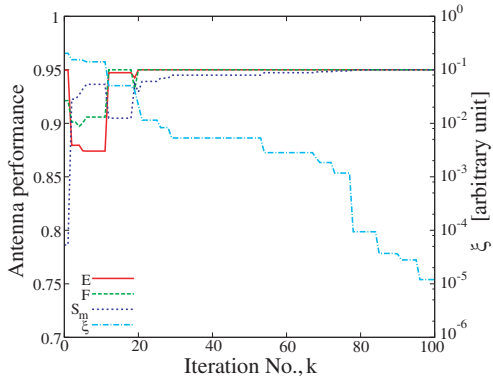

Figure 5. *Test Case A* — Evolution of the cost function ξ and of the antenna performance indexes (antenna efficiency E, system fidelity F, and similarity factor S).

Table 1. *Test Case A* — Descriptive parameters.

Geometric Variables [mm]						
α_1		α_2		α_3		α_4
30.1		8.1		3.9		11.0
Control Ponits Coordinates [mm]						
P_1	P_2	P_3	P_4	P_5	P_6	P_7
(3.9, 17.2)	(4.5, 18.5)	(4.8, 19.6)	(4.1, 24.8)	(2.7, 21.2)	(2.1, 21.7)	(0.0, 19.0)
Q_1	Q_2	Q_3	Q_4	Q_5	Q_6	Q_7
(3.2, 0.0)	(1.4, 1.5)	(5.3, 3.8)	(3.2, 3.5)	(3.1, 5.0)	(2.8, 5.8)	(8.1, 2.9)

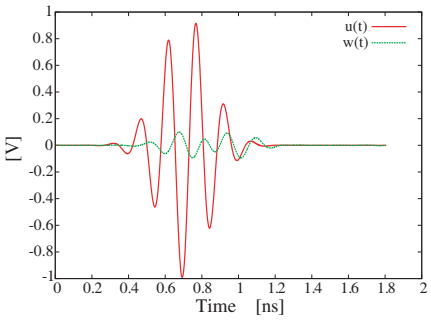

Figure 6. *Test Case A* — Input signal $u(t)$ and reflected signal $w(t)$.

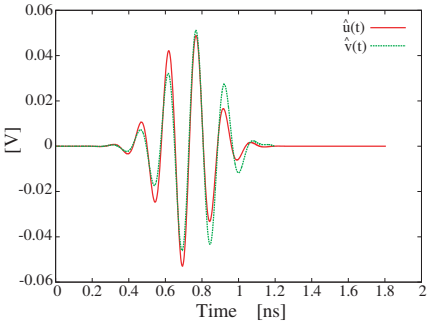

Figure 7. *Test Case A* — Energy-normalized input signal $\hat{u}(t)$ and energy normalized received signal $\hat{v}(t)$.

behavior has been described in terms scattering parameters. Simulated and measured s_{11} and s_{21} values are shown in Fig. 9. For the experimental validation, the synthesized antenna has been realized on an Arlon dielectric substrate ($\epsilon_r = 3.38$) of thickness 0.78 mm by using the photolitographic printing circuit technology. The prototype (Fig. 10) has been equipped with a SMA connector and fed with a coaxial cable at ($y_{\text{feed}} = 0.0$, $z_{\text{feed}} = \alpha_4$) to allow a set of measurements with a Vector Network Analyzer in an anechoic chamber.

Besides a reasonable agreement between simulated and measured data, the s_{11} magnitude turns out to be smaller than -10 dB in a wide portion of the frequency spectrum from 4 GHz up to 9 GHz [Fig. 9(a)] confirming the indications drawn from the analysis of the efficiency value ($E = 0.98$) and the arising amplitude of $w(t)$. Moreover, the magnitude of s_{21} presents reduced variations always smaller than 7 dB

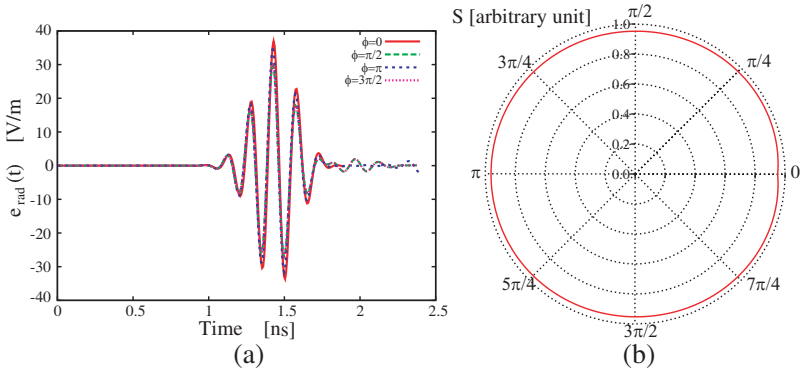

Figure 8. *Test Case A* — Radiated electric field (a) and similarity factor values (b).

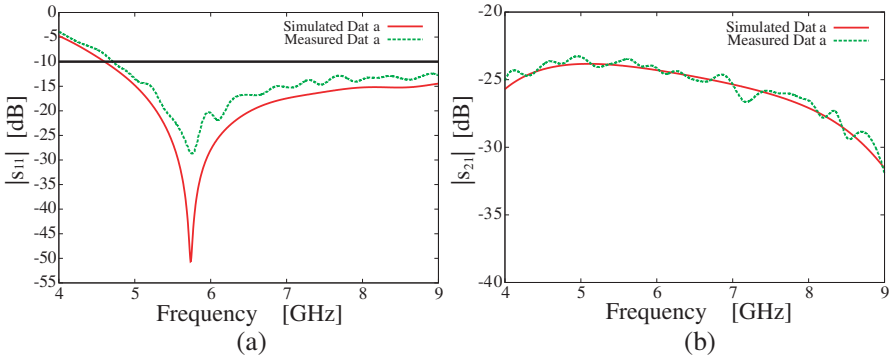

Figure 9. *Test Case A* — Magnitude of the (a) s_{11} and (b) s_{21}.

Figure 10. *Test Case A* — Antenna prototype.

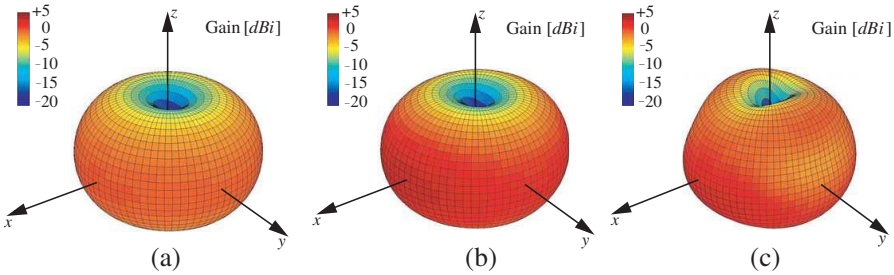

Figure 11. *Test Case A* — Total gain radiation patterns at (a) $f = 4\,\text{GHz}$, (b) $f = 6.5\,\text{GHz}$, and (c) $f = 9\,\text{GHz}$.

that guarantee a non-distorted reception of the transmitted UWB pulses as previously suggested by the plot in Fig. 7 and confirmed by the value of the system fidelity index ($F = 0.97$).

Still in the frequency domain, the radiation features of the synthesized antenna have been also analyzed. Fig. 11 shows the simulated three-dimensional radiation patterns of the total gain at $f = 4\,\text{GHz}$, $f = 6.5\,\text{GHz}$, and $f = 9\,\text{GHz}$. The antenna behaves like an omnidirectional radiator along the horizontal plane (x-y plane) as deduced from the similarity factor analysis (Fig. 8). Analogously to conventional dipole antennas, two nulls appear in the radiation patters along the z-axis as it can be also observed in Fig. 12 where numerical data and experimental values of the total gain along the horizontal and vertical planes are compared.

The second test case (*Test Case B*) deals with the synthesis of a UWB system operating in a lower band from 2.5 GHz up to 5.5 GHz with the radiators spaced by $d = 30\,\text{cm}$. In such a case, the target indexes have been set to $E^T = F^T = 0.95$ and $S^T(\theta, \phi) = 0.92$ ($\theta = 90°$), while the antenna has been constrained to an area not larger than $80 \times 60\,\text{mm}^2$. The PSO parameters have been kept unaltered from the *Test Case A*, and consequently the overall time required by the optimization has been approximately the same. Regarding the antenna geometry, it has been parametrized with $I = 8$ and $J = 5$ control points (i.e., $N = 30$).

After the optimization, the antenna descriptors turned out to be set at the values in Table 2 and the prototype of the optimized antenna is as shown in Fig. 13 with a size of $68.7 \times 38.8\,\text{mm}^2$.

As for the antenna performances, the efficiency index results equal to $E = 0.97$ as required to guarantee a reliable communication without strong reflections. This is confirmed by the plots in Fig. 14 and in Fig. 15 where the reflected $w(t)$ and the received $v(t)$ signals are compared with the input waveform $u(t)$, respectively. As for this

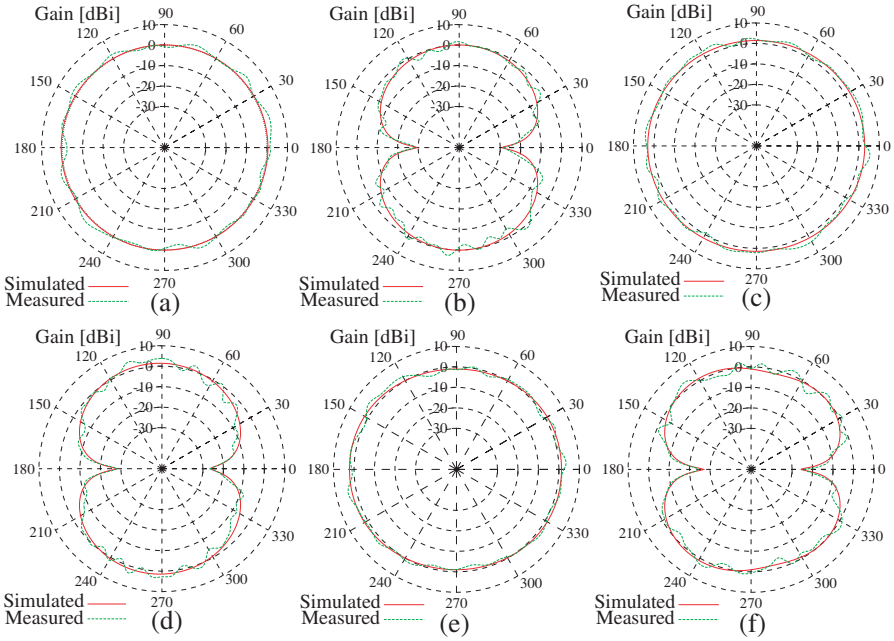

Figure 12. *Test Case A* — Simulated and measured total gain values at (a) (b) $f = 4\,\text{GHz}$, (c) (d) $f = 6.5\,\text{GHz}$, and (e) (f) $f = 9\,\text{GHz}$ along (a) (c) (e) the horizontal ($\theta = 90°$) and (b) (d) (f) the vertical plane ($\phi = 90°$).

Table 2. *Test Case B* — Descriptive parameters.

Geometric Variables [mm]							
α_1		α_2		α_3		α_4	
68.7		19.4		2.1		16.8	
Control Ponits Coordinates [mm]							
P_1	P_2	P_3	P_4	P_5	P_6	P_7	P_8
(2.1, 18.3)	(7.2, 18.8)	(13.4, 19.2)	(5.5, 22.4)	(6.7, 24.4)	(16.4, 28.5)	(9.7, 31.8)	(0.0, 42.6)
Q_1		Q_2		Q_3	Q_4	Q_5	
(16.6, 0.0)		(12.7, 9.0)		(13.4, 12.6)	(8.0, 13.7)	(19.4, 14.2)	

latter comparison, it can be observed that the agreement between transmitted and received waveforms turns out to be slightly worse than in the previous test case because of the smaller fidelity index ($F = 0.95$ vs. $F = 0.97$) even though acceptable and within the project constraints.

Concerning the time-domain analysis of the antenna radiation,

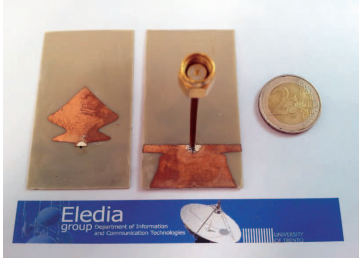

Figure 13. *Test Case B* — Antenna prototype.

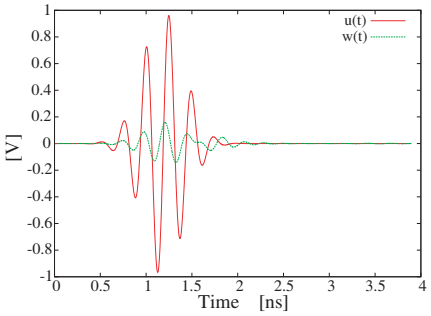

Figure 14. *Test Case B* — Input signal $u(t)$ and reflected signal $w(t)$.

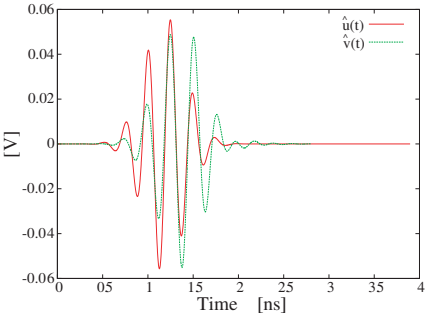

Figure 15. *Test Case B* — Energy-normalized input signal $\hat{u}(t)$ and energy normalized received signal $\hat{v}(t)$.

Fig. 16 shows the time behavior of the radiated field in different ϕ directions and the arising similarity factor. Likewise the '*Test Case A*', the antenna exhibits an omnidirectional behavior along the horizontal plane with $S(\theta = 90^o, \phi) > 0.92$.

As far as the frequency-domain study is concerned, Fig. 17 gives an overview of the behaviour of the electric parameters. As it can be drawn from Fig. 17(a), there is a good impedance matching with s_{11} magnitudes generally smaller than $-10\,\mathrm{dB}$ ($E = 0.97$). Unlike the previous test case and as suggested from the lower value of F ($F = 0.95$ vs. $F = 0.97$), slightly more significant variations of s_{21} arise [Fig. 17(b)].

Finally, Fig. 18 shows the simulated three-dimensional dipole-like patterns of the synthesized antenna at $f = 2.5\,\mathrm{GHz}$, $f = 4\,\mathrm{GHz}$, and $f = 5.5\,\mathrm{GHz}$, while the results of a consistency check between simulations and measurements are reported in Fig. 19.

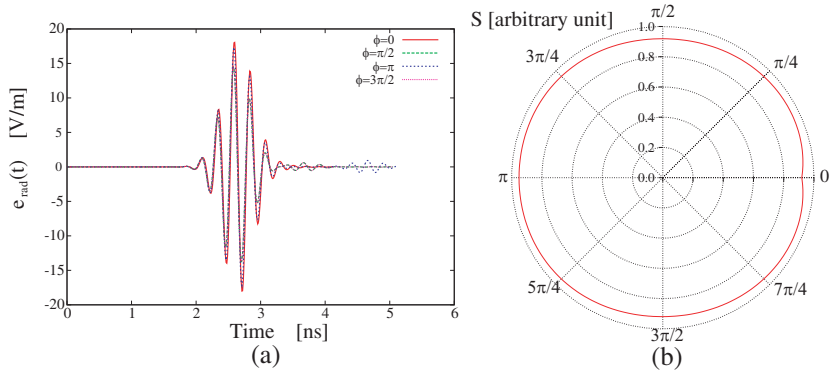

Figure 16. *Test Case B* — (a) Radiated electric field and (b) similarity factor values.

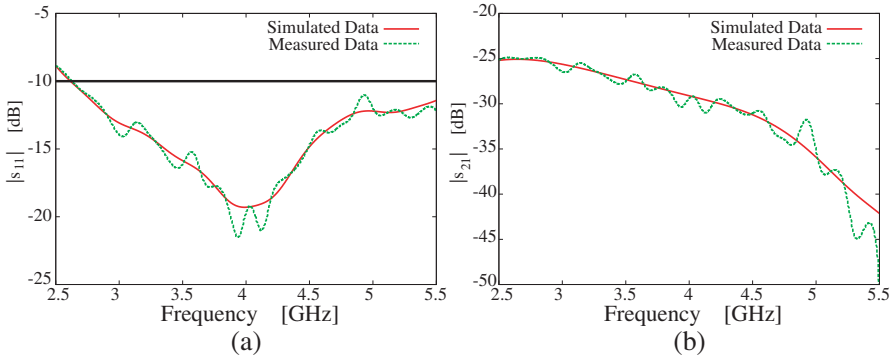

Figure 17. *Test Case B* — Magnitude of (a) s_{11} and (b) s_{21}.

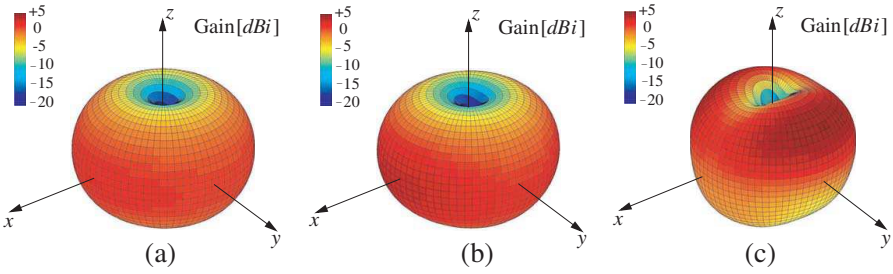

Figure 18. *Test Case B* — Total gain radiation patterns at (a) $f = 2.5\,\text{GHz}$, (b) $f = 4\,\text{GHz}$, and (c) $f = 5.5\,\text{GHz}$.

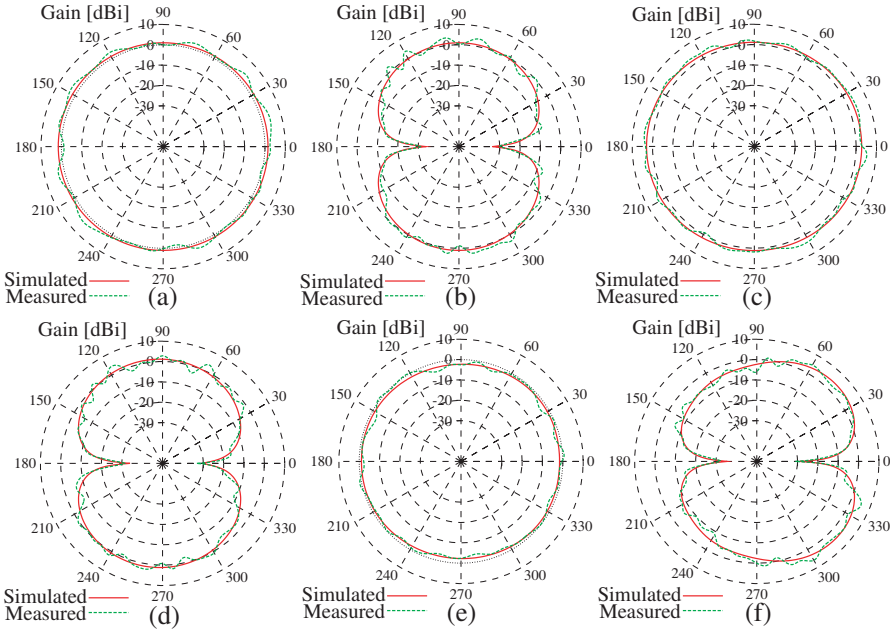

Figure 19. *Test Case B* — Total gain radiation patterns at (a) $f = 2.5\,\text{GHz}$, (b) $f = 4\,\text{GHz}$, and (c) $f = 5.5\,\text{GHz}$. *Test Case B* — Simulated and measured total gain values at (a) (b) $f = 2.5\,\text{GHz}$, (c) (d) $f = 4\,\text{GHz}$, and (e) (f) $f = 5.5\,\text{GHz}$ along the (a) (c) (e) horizontal ($\theta = 90°$) and (b) (d) (f) vertical plane ($\phi = 90°$).

5. CONCLUSIONS

In this paper, an approach entirely in time-domain for the synthesis of a UWB radiating system has been presented. Starting from a spline-based description of the antenna structure, the design process has been recast as a time-domain optimization carried out by means a PSO-based iterative approach. In order to assess the effectiveness of the proposed technique, both numerical and experimental results have been presented and discussed. Besides the agreement between simulations and measurements, which confirms the reliability of the proposed numerical method, the results provide solid proofs about the efficiency of the proposed methodology in synthesizing UWB antenna systems.

REFERENCES

1. Arslan, H., Z. N. Chen, and M. Di Benedetto, *Ultra Wideband Wireless Communication*, Wiley, Hoboken, NJ, 2006.
2. Carro, P. L. and J. de Mingo, "Ultrawide-band antenna distortion characterization using hermite-gauss signal subspace," *IEEE Antennas Wireless Propag. Lett.*, Vol. 7, 267–270, 2008.
3. Zhang, Z. and Y. H. Lee, "A robust cad tool for integrated design of UWB antenna system," *Progress In Electromagnetics Research*, Vol. 112, 441–457, 2011.
4. Balanis, C. A., *Antenna Theory: Analysis and Design*, Wiley, New York, 1996.
5. Soergel, W. and W. Wiesbeck, "Influence of the antennas on the ultra-wideband transmission," *EURASIP J. on Appl. Signal Process.*, No. 3, 296–305, 2005.
6. Dadgarnia, A. and A. A. Heidari, "A fast systematic approach for microstrip antenna design and optimization using ANFIS and GA," *Journal of Electromagnetic Waves and Applications*, Vol. 24, No. 16, 2207–2221, 2010.
7. Bialkowski, M. E. and A. M. Abbosh, "Design of UWB planar antenna with improved cut-off at the out-of-band frequencies," *IEEE Antennas Wireless Propag. Lett.*, Vol. 7, 408–410, 2008.
8. Pergol, M. and W. Zieniutycz, "Unified design procedure for planar dipoles oriented on UWB application," *Progress In Electromagnetics Research*, Vol. 102, 249–265, 2010.
9. Gopikrishna, M., D. Das Krishna, C. K. Anandan, P. Mohanan, and K. Vasudevan, "Design of a compact semi-elliptic monopole slot antenna for UWB systems," *IEEE Trans. on Antennas and Propag.*, Vol. 57, No. 6, 1834–1837, 2009.
10. Lizzi, L., F. Viani, R. Azaro, and A. Massa, "A PSO-driven spline-based shaping approach for ultra-wideband (UWB) antenna synthesis," *IEEE Trans. on Antennas and Propag.*, Vol. 56, No. 8, 2613–2621, 2008.
11. Farr, G. and C. E. Baum, "Extending the definitions of antenna gain and radiation pattern into the time domain," *Sensor Sim. Notes*, Note 350, 1992.
12. Akhoondzadeh-Asl, L., M. Fardis, A. Abolghasemi, and G. R. Dadashzadeh, "Frequency and time domain characteristic of a novel notch frequency UWB antenna," *Progress In Electromagnetics Research*, Vol. 80, 337–348, 2008.
13. Karousos, A. and C. Tzaras, "Multiple time-domain diffraction for

UWB signals," *IEEE Trans. on Antennas and Propag.*, Vol. 56, No. 5, 1420–1427, 2008.

14. Barbarino, S. and F. Consoli, "UWB circular slot antenna provided with an inverted-L notch filter for the 5 GHz WLAN band," *Progress In Electromagnetics Research*, Vol. 104, 1–13, 2010.
15. Lamensdorf, D. and L. Susman, "Baseband-pulse-antenna techniques," *IEEE Antennas Propag. Magazine*, Vol. 36, No. 1, 20–30, 1994.
16. Franceschetti, G., J. Tatoian, and G. Gibbs, "Timed arrays in a nutshell," *IEEE Trans. on Antennas and Propag.*, Vol. 53, No. 12, 4073–4082, 2005.
17. Shlivinski, A., E. Heyman, and R. Kastner, "Antenna characterization in the time domain," *IEEE Trans. on Antennas and Propag.*, Vol. 45, No. 7, 1140–1149, 1997.
18. Telzhensky, N. and Y. Leviatan, "Novel method of UWB antenna optimization for specified input signal forms by means of genetic algorithm," *IEEE Trans. on Antennas and Propag.*, Vol. 54, No. 8, 2216–2225, 2206.
19. Telzhensky, N. and Y. Leviatan, "Planar differential elliptical UWB antenna optimization," *IEEE Trans. on Antennas and Propag.*, Vol. 54, No. 11, 3400–3406, 2206.
20. Li, Z. Q., C. L. Ruan, and L. Peng, "Design and analysis of planar antenna with dual WLAN band-notched for integrated bluetooth and UWB applications," *Journal of Electromagnetic Waves and Applications*, Vol. 24, No. 13, 1817–1828, 2010.
21. Robinson, J. and Y. Rahmat-Samii, "Particle swarm optimization in electromagnetics," *IEEE Trans. on Antennas and Propag.*, Vol. 52, 397–407, 2004.
22. Mikki, S. M. and A. A. Kishk, "Physical theory for particle swarm optimization," *Progress In Electromagnetics Research*, Vol. 75, 171–207, 2007.
23. Benedetti, M., G. Oliveri, P. Rocca, and A. Massa, "A fully-adaptive smart antenna prototype: Ideal model and experimental validation in complex interference scenarios," *Progress In Electromagnetics Research*, Vol. 96, 173–191, 2009.
24. Rocca, P., M. Benedetti, M. Donelli, D. Franceschini, and A. Massa, "Evolutionary optimization as applied to inverse scattering problems," *Inverse Probl.*, Vol. 25, No. 12, 1–41, 2009.
25. De Boor, C., *A Practical Guide to Spline*, Springer, New York, 2001.

26. Lin, C. C., Y. C. Kan, L. C. Kuo, and H. R. Chuang, "A planar triangular monopole antenna for UWB communication," *IEEE Microw. Wireless Compon. Lett.*, Vol. 15, No. 10, 624–626, 2005.
27. Liang, J., C. C. Chiau, X. Chen, and C. G. Parini, "Study of a printed circular disc monopole antenna for UWB systems," *IEEE Trans. on Antennas and Propag.*, Vol. 53, No. 11, 3500–3504, 2005.
28. Johnson, J. M. and Y. Rahmat-Samii, "Genetic algorithms and method of moments (GA/MoM) for the design of integrated antennas," *IEEE Trans. on Antennas and Propag.*, Vol. 47, No. 10, 1606–1614, 1999.
29. Villegas, F. J., T. Cwik, Y. Rahmat-samii, and M. Manteghi, "A parallel electromagnetic genetic-algorithm optimization (EGO) application for patch antenna design," *IEEE Trans. on Antennas and Propag.*, Vol. 52, No. 9, 2424–2435, Sep. 2004.
30. Lizzi, L., G. Oliveri, and A. Massa, "Exploitation of spline-based geometries for the time-domain synthesis of UWB antennas," *Proc. 5th European Conf. Antennas Propagation (EuCAP)*, 2382–2385, Rome, Italy, Apr. 11–15, 2011.
31. Carlson, A. B., P. B. Crilly, and J. C. Rutledge, *Communication Systems*, McGraw-Hill, New York, 2002.
32. Benedetti, M., R. Azaro, D. Franceschini, and A. Massa, "PSO-based real- time control of planar uniform circular arrays," *IEEE Antennas Wireless Propag. Lett.*, Vol. 5, 545–548, 2006.
33. Benedetti, M., R. Azaro, and A. Massa, "Memory enhanced PSO-based optimization approach for smart antennas control in complex interference scenarios," *IEEE Trans. on Antennas and Propag.*, Vol. 56, No. 7, 1939–1947, 2008.
34. Azaro, R., F. Caramanica, and G. Oliveri, "Determination of the complex permittivity values of planar dielectric substrates by means of a multifrequency PSO-based technique," *Progress In Electromagnetics Research M*, Vol. 10, 83–91, 2009.
35. Van Rienen, U., *Numerical Methods in Computational Electrodynamics: Linear Systems in Practical Applications*, Springer, New York, 2001.
36. Poli, L., P. Rocca, L. Manica, and A. Massa, "Handling sideband radiations in time-modulated arrays through particle swarm optimization," *IEEE Trans. on Antennas and Propag.*, Vol. 58, No. 4, 1408–1411, 2010.